

Embedding Neighborhoods Simultaneously t-SNE (ENS-t-SNE)

Vahan Huroyan, Raymundo Navarrete, Md Iqbal Hossain, Stephen Kobourov

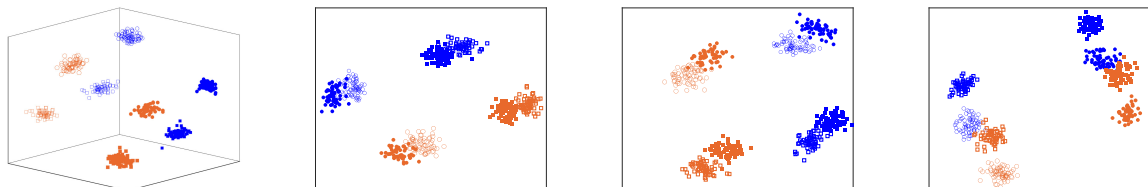


Fig. 1: The ENS-t-SNE embedding of a 400-point dataset with three perspectives: in each perspective there are two clusters. The dataset is created as follows: half of the points are randomly assigned to one group and the other half to the other group. The distance between points within the same group is 1 (plus small Gaussian noise) while the distance between points in different groups is 2 (plus small Gaussian noise). The left figure shows one view of the 3D ENS-t-SNE embedding; the next three figures show the corresponding three projections. The original clusters are shown in color (blue, orange), shape (square or circle) and texture (filled or not). The ENS-t-SNE algorithm recovers the clusters and creates an embedding which respects all 3 types of clusters simultaneously.

Abstract— We propose an algorithm for visualizing a dataset by embedding it in 3-dimensional Euclidean space based on various given distances between the same pairs of datapoints. Its aim is to find an Embedding which preserves Neighborhoods Simultaneously for all given distances by generalizing the t-Stochastic Neighborhood Embedding approach (ENS-t-SNE). We illustrate the utility of ENS-t-SNE by demonstrating its use in three applications. First, to visualize different notions of clusters and groups within the same high-dimensional dataset with one 3-dimensional embedding, as opposed to providing different embeddings of the same data and trying to match the corresponding points. Second, to illustrate the effects of different hyper-parameters of the classical t-SNE. Third, by considering multiple different notions of clustering in data, ENS-t-SNE can generate an alternative embedding than the classic t-SNE. We provide an extensive quantitative evaluation with real-world and synthetic datasets of different sizes and using different numbers of projections.

Index Terms—Graph visualization, Dimensionality reduction, t-SNE, Multidimensional scaling, Mental map preservation.

1 Introduction

Visualizing a high-dimensional dataset is one of the main applications of dimensionality reduction and many different methods have been proposed over the years. Some of the most popular ones include the Principal Component Analysis (PCA) [16], Multi-Dimensional Scaling (MDS) [25], Laplacian Eigenmaps [2], t-Distributed Stochastic Neighbor Embedding (t-SNE) [20], and Uniform Manifold Approximation and Projection (UMAP) [22]. Depending on the task, these algorithms preserve different characteristics of the dataset while embedding it into a lower dimensional space. Some of these algorithms, such as PCA and MDS aim to preserve the global distances, while others such as t-SNE, Laplacian Eigenmaps, Diffusion Maps, and UMAP aim to preserve the local information of the dataset.

In real-world applications, when trying to visualize a high dimensional dataset, the goal is usually to place datapoints with similar features together and datapoints with different features far from each other. In recent years, several non-linear dimensionality reduction algorithms [20, 22] focused on finding an embedding of the dataset in lower dimensional spaces which

would preserve these local structures. In other words, the goal is to have an embedding of the dataset in a lower dimensional space, such that the datapoints that are close to each other in a given higher dimensional space are also close to each other in the embedded space. Two successful and widely used algorithms for this task include t-SNE [20] and UMAP [22, 12]. These algorithms have found many successful applications in various fields; see the recent survey [12].

High dimensional datasets capture information about the same object or phenomenon from many sources/sensors. Simply concatenating this information into one vector per datapoint might not always be appropriate, because each might have its specific statistical property and interpretation. Therefore, methods to visualize and analyze such datasets, in a way that allows us to see multiple types of relationships between the datapoints are needed. Standard 2-dimensional space might not be enough to simultaneously capture and show various relationships between the datapoints. Instead we propose to embed the dataset in 3D and use different perspectives (or view-points, or projections) to present the desired information. Hossain et al. [15] first used 3D space for multi-perspective simultaneous embedding, where the goal was to capture global distances between the datapoints. In this work we focus on preserving local relationships, i.e., we aim to preserve the local neighborhoods and pay less attention to points that are far from each other. More formally, we consider the following problem: Given various relationships (distance matrices/dissimilarity matrices) between the same set of datapoints, find a 3D embedding of these datapoints along with the corresponding 2D projections such that these projections preserve the given relationships; see Figure 1. Our algorithm for Embedding Neighborhoods Simul-

• Vahan Huroyan and Raymundo Navarrete are with the Department of Mathematics of The University of Arizona, E-mails: vahanhuroyan@math.arizona.edu and raymundo@math.arizona.edu.

• Md Iqbal Hossain and Stephen Kobourov are with the Computer Science Department of The University of Arizona, E-mails: hossain@email.arizona.edu and kobourov@cs.arizona.edu.

taneously t-SNE (ENS-t-SNE) becomes just t-SNE [20] in the case when only a single relationship is taken into account.

1.1 Previous Work

In this section we review related work in dimensionality reduction, multi-view embeddings, and visualization.

Multi-Dimensional Scaling (MDS) [25]. MDS solves the following problem: Given a set of distances between N objects, embed a set of N points in \mathbb{R}^p (for visualization purposes the standard choice of p is 2 or 3) such that the distances between these embedded points are as close to the given distances as possible. This method is also used for dimensionality reduction purposes, where instead of distances between objects we are given a set of datapoints in high dimensional space and the goal is to embed the dataset in lower dimensions such that the distances in the embedded space are as close to the distances in the original space as possible.

Mathematically, the problem is formulated as follows: Given a set of pairwise distances D_{ij} between N objects $1 \leq i, j \leq N$, MDS aims to assign coordinates $y_1, y_2, \dots, y_N \in \mathbb{R}^p$ such that the distances $\|y_i - y_j\|$ closely approximate the original pairwise distances D_{ij} . The original pairwise distances are given by an $N \times N$ matrix D . To solve this problem MDS uses the following objective function, which is known as the stress function:

$$\sigma^2(Y) = \sum_{i>j} (D_{ij} - \|y_i - y_j\|)^2. \quad (1)$$

The goal is find an embedding $Y = [y_1, y_2, \dots, y_N]$ in the low-dimensional space so that the stress function σ^2 is minimized. The stress function is non-convex. Thus, it is hard to find guarantees that standard optimization techniques will always solve the minimization problem.

Minimizing the stress function (1) is typically accomplished using gradient or stochastic gradient descent methods [6]. Another method for solving MDS optimization problem is by stress majorization [10]. We remark that the original formulation of multidimensional scaling is non-metric MDS. The problem was first studied in the non-metric setting by Shepard [25] and Kruskal [18]. Non-metric MDS recovers structure from measures of similarity, based on the assumption of a reproducible ordering between the distances, rather than relying on the exact distances.

Principal Component Analysis (PCA) [16]. PCA is a widely used dimensionality reduction technique. The goal is to increase the interpretability of the dataset but at the same time minimize the information loss. PCA aims to preserve as much variance of the dataset as possible in the lower dimensional embedding. The principal components of a given dataset can be computed by eigen-decomposition of the data’s covariance matrix, or by singular value decomposition of the data matrix.

T-Distributed Stochastic Neighbor Embedding (t-SNE). Another method to visualize a high-dimensional data in scatter plots is t-Distributed Stochastic Neighbor Embedding (t-SNE) [20, 27]. Similar to MDS, t-SNE produces an embedding that closely represents distances in the samples, but instead of using the stress function it uses a cost function that better preserves local and cluster distances and ignores distances between samples that are far apart. Given a distance or dissimilarity matrix \mathbf{D}_{ij} or a high dimensional dataset $x_1, \dots, x_N \in \mathbb{R}^D$ t-SNE aims to embed this dataset in a lower dimensional space \mathbb{R}^p such that the neighborhood information of the dataset is preserved. That is, if two points are neighbors in the original space, they should be neighbors in the embedded space as well.

The mathematical formulation of the problem is the following: Given an $N \times N$ distance matrix D , one can construct the $N \times N$ distance matrix from a given dataset by just considering the Euclidean distances between them, and a perplexity

parameter, t-SNE seeks to minimize the following cost function:

$$C(Y) = \sum_{i,j} p_{i|j} \log \frac{p_{i|j}}{q_{i|j}} \quad (2)$$

Here, $P = [p_{i|j}]$ is determined by D and the perplexity parameter and $Q = [q_{i|j}]$ is a function of Y . More explicitly, $p_{ij}^m = p_{ji}^m + p_{i|j}^m$, where

$$p_{i|i} = \frac{e^{-(D_{ij})^2/2(\sigma_i)^2}}{\sum_{k \neq i} e^{-(D_{ik})^2/2(\sigma_i)^2}} \quad (3)$$

and

$$q_{i|i} = \frac{(1 + \|\Pi(y_i - y_j)\|^2)^{-1}}{\sum_{k \neq i} (1 + \|\Pi(y_k - y_i)\|^2)^{-1}}. \quad (4)$$

The computational complexity of t-SNE is high and some speed improvements have been proposed [26]. Although the original paper proposes default values and ranges for the t-SNE hyperparameters (perplexity, learning rate, etc.), automatically selecting these parameters is also a topic of interest [8, 3]. A recent paper reviews t-SNE and applications thereof [11].

Uniform Manifold Approximation and Projection (UMAP) Similar to t-SNE, Uniform Manifold Approximation and Projection (UMAP) [22, 21] is another non-linear dimensionality reduction method that aims to preserve local distances. Some advantages of UMAP over the other non-linear dimensionality reduction algorithms include the ability to use labels (or partial labels) for supervised or semi-supervised dimensionality reduction. Moreover, it allows one to transform new unseen data into a pre-trained embedding space. A review of different variants of UMAP and its applications is summarized in [12].

Simultaneous Embedding. The problem of simultaneous embedding is related to several fields, such as simultaneous graph embedding, matched drawings of graphs [5], and simultaneous matrix orderings for graph collection [4]. For example, simultaneous geometric embedding of two or more planar graphs requires planar straight-line drawings of each of the graphs, such that common vertices have the same 2D coordinates in all drawings [7]. Matched drawings require straight-line drawings of the two or more input graphs such that each common vertex has the same y -coordinate in all drawings [13]. In a different setting of simultaneous embedding [4] consider simultaneous matrix orderings for graph collection, where for a given set of graphs, the goal is to compute a single ordering that works well for visualizing each graph as a matrix.

Some recent algorithms for simultaneous embedding/multiview embedding include: Multiview Stochastic Neighbor Embedding (m-SNE) [29, 30] and Multiview Spectral Embedding (MSE) [28]. The m-SNE [29, 30] is based on a probabilistic framework that integrates heterogeneous features of the dataset into one combined embedding. The MSE [28] is a spectral-embedding algorithm, which encodes features in such a way to achieve a physically meaningful embedding. The MSE is an optimization-based iterative algorithm which finds a low dimensional embedding such that the distribution of each view is sufficiently smooth, and that the MSE explores the complementary property of different views.

Multi-view Data Visualisation via Manifold Learning [24], proposes extensions of t-SNE, LLE and ISOMAP, for dimensionality reduction and visualisation of multiview data by computing and summing together the gradient descent for each data-view. Multi-view clustering for multi-omics data using unified embedding [23] uses the sum of Kullback-Leibler divergence over the datapoints, which leads to a simple gradient adjusting the position of the samples in the embedded space. Our proposed algorithm finds the low dimensional embedding as well as the corresponding perspectives/views under which

the particular distance matrix is visualized by preserving the local information.

Multi-View Multidimensional Scaling. As we have already discussed, for a single pairwise distance or dissimilarity matrix \mathbf{D} , MDS aims to find an embedding X that minimizes MDS stress function in (1). However, in various applications, data might be collected from various sources or by various sensors resulting in *multiple* dissimilarity matrices. Thus, the following extension of the MDS is natural: Given K dissimilarity matrices $\mathcal{D} = \{\mathbf{D}^1, \mathbf{D}^2, \dots, \mathbf{D}^K\}$ for the same N objects, how to construct an embedding X that best represents all of these dissimilarities simultaneously? If we assume that the different dissimilarity matrices correspond to different noisy measurements. One simple solution can be to consider the average of these measurements. That is, consider the average $(\mathbf{D}^1 + \mathbf{D}^2 + \dots + \mathbf{D}^K)/K$ is an estimate of \mathbf{D} . It would then be possible to construct an MDS embedding using the estimate of \mathbf{D} . Another alternative is to construct an embedding directly, by finding an embedding X that best approximates all of the pairwise dissimilarities simultaneously, for example, by solving the following optimization problem:

$$\sum_{k=1}^K \sigma^2(\mathbf{X}; \mathbf{D}^k) = \sum_{k=1}^K \sum_{i>j} \left(\mathbf{D}_{ij}^k - \|x_i - x_j\| \right)^2.$$

Bai et. al [1] propose finding the embedding \mathbf{X} that minimizes the Multi-View Multidimensional Scaling (MVMD) stress function

$$S_{MV}(\mathbf{X}, \alpha; \mathcal{D}) = \sum_{k=1}^K \alpha_k^\gamma \sum_{i<j} \left(\mathbf{D}_{ij}^k - \|x_i - x_j\| \right)^2,$$

where the weights $\alpha = [\alpha_1, \alpha_1, \dots, \alpha_K]$ are subject to the constraints $\sum_{k=1}^K \alpha_k = 1$, $0 \leq \alpha_k \leq 1$, and $\gamma > 1$ is a fixed parameter. Here the objective is to find an embedding X that minimizes a weighted sum of the MDS stress (1) for the different dissimilarity matrices. The parameter γ balances between just finding the embedding that produces the smallest single stress $\sigma^2(\mathbf{X}; \mathbf{D}^k)$ and assigning equal weights to all of the individual stress values. This idea, along with similar multi-view generalizations of other visualization algorithms, are implemented by Kanaan et al. [17].

Multi-Perspective Simultaneous Embedding (MPSE). In the approaches described under Multi-view multidimensional scaling, the assumption is that the given dissimilarity/distance matrices measure the same relationship in the data with possible errors. However, it is possible that the different dissimilarity matrices measure different relationships in the data. MPSE aims to find an embedding of a graph, such that the different perspectives $P^k(X)$ of the embedding X can visualize the different dissimilarities \mathbf{D}^k simultaneously [15].

The MPSE algorithm can be seen as a generalization of MDS that is able to visualize multiple distance matrices simultaneously, by producing a three-dimensional embedding, so that the different distance matrices are preserved after projecting the 3D coordinates to 2D ones using specified projections. Given a set of M $N \times N$ distance matrices D^1, D^2, \dots, D^M , MPSE aims to find 3D coordinates x_1, x_2, \dots, x_N for the samples $i = 1, 2, \dots, N$ and a set of 3D to 2D projection matrices $\Pi^1, \Pi^2, \dots, \Pi^M$ so that

$$\sigma_M^2(X, \Pi) = \sum_{m=1}^M \sigma^2(\Pi^m X) \quad (5)$$

where σ^2 is the MDS stress function (1). While MPSE optimizes global distances (as it generalizes MDS), the algorithm proposed here, ENS-t-SNE, optimizes local distances (as it generalizes t-SNE).

2 Embedding Neighborhoods Simultaneously

Our proposed ENS-t-SNE algorithm is a generalization of the standard t-SNE algorithm. For ENS-t-SNE, we assume a set of distance matrices for the same set of objects. Similar to Multi-Perspective Simultaneous Embedding [15], where the goal was to generalize the MDS in order to achieve a multi-perspective visualization of a dataset that would preserve distances for corresponding projections, we generalize t-SNE. For this purpose we generalize the objective function of t-SNE onto the one that would take multiple distance matrices and have one projection for each on which the desired distances would locally be preserved. We generalize the objective function of t-SNE as follows: Assume we are given M distance matrices between n objects. We define

$$\tilde{C} = \sum_{m=1}^M \sum_i \sum_j p_{ij}^m \log \frac{p_{ij}^m}{q_{ij}^m} \quad (6)$$

where $p_{j|i}^m$ and q_{ij}^m for $1 \leq i, j \leq N$ and $1 \leq m \leq M$ are defined as

$$p_{j|i}^m = \frac{e^{-(D_{ij}^m)^2/2(\sigma_i^m)^2}}{\sum_{k \neq i} e^{-(D_{ik}^m)^2/2(\sigma_i^m)^2}}, \text{ and } p_{ij}^m = p_{j|i}^m + p_{i|j}^m, \quad (7)$$

and

$$q_{ij}^m = \frac{(1 + \|\Pi^m(y_i - y_j)\|)^{-1}}{\sum_{k \neq l} (1 + \|\Pi^m(y_k - y_l)\|)^{-1}}. \quad (8)$$

Here D_{ij}^m for $1 \leq i, j \leq n$ corresponds to the m -th distance matrix between objects i and j , Π^m corresponds to the m -th projection, which depending on the problem might be given or not, and y_1, \dots, y_N correspond to the desired embedding. The objective function \tilde{C} is a function of the embedding y_1, \dots, y_N and projections Π^1, \dots, Π^M . The goal is to find y_1, \dots, y_N and Π^1, \dots, Π^M that would minimize \tilde{C} . The only parameter that we have not discussed yet are the σ_i^m . These parameters are application specific and can vary depending on the dataset. Depending on the density of the dataset around each high dimensional point, the values of σ_i^m can vary. The denser the dataset is, the smaller σ_i^m can be chosen to be.

In order to pick appropriate values for σ_i^m for all $1 \leq i \leq N$ and $1 \leq m \leq M$, we follow the steps of [20] and use the notion of perplexity. Perplexity can be interpreted as a smooth measure of the effective number of neighbors to consider. Each value of σ_i^m creates a new distribution P_i^m over the datapoints. Similar to t-SNE we perform a binary search to compute the value of σ_i^m that produces a distribution P_i^m with a fixed perplexity that is specified by the user. The perplexity is defined as

$$\text{Perp}(P_i^m) = 2^{H(P_i^m)}, \quad (9)$$

where $H(P_i^m)$ is the Shannon entropy function, defined as

$$H(P_i^m) = - \sum_j p_{j|i}^m \log_2(p_{j|i}^m). \quad (10)$$

In order to optimize the objective function of ENS-T-SNE (6) we use stochastic gradient descent discussed in Sec. 2.1. We would like to mention that one can compute the exact gradients of \tilde{C} .

There are two natural variants of this problem. The first version assumes that we are given a set of projections Π^1, \dots, Π^M and a set of distance matrices $D^1, \dots, D^M \in \mathbb{R}^{N \times N}$ between N objects, where each projection matrix corresponds to one distance matrix. The goal is to find an embedding of the dataset in 3D $Y = \{y_1, \dots, y_N\}$ such that on each of these projections the corresponding distances are locally preserved. The second version assumes only a set of distance matrices $D^1, \dots, D^M \in$

$\mathbb{R}^{N \times N}$ and finds the best embedding $Y = \{y_1, \dots, y_N\}$ as well as the projections Π^1, \dots, Π^M onto which the local distances would be preserved.

2.1 ENS-T-SNE Algorithm

In this section we summarize the ENS-T-SNE algorithm and provide a practical implementation. Given a list of $N \times N$ distance matrices D^1, D^2, \dots, D^M and a perplexity parameter Perp, ENS-T-SNE algorithm aims to find a three-dimensional embedding $x_1, x_2, \dots, x_N \in \mathbb{R}^3$ and a set of projection matrices $\Pi^1, \Pi^2, \dots, \Pi^M \in \mathbb{R}^{2 \times 3}$ so that for each perspective $m = 1, 2, \dots, M$, the corresponding projected dataset $\Pi^m x_1, \Pi^m x_2, \dots, \Pi^m x_M$ minimizes the t-SNE cost function $C(Y^m)$ on that particular 2D Euclidean space as much as possible.

We write $X = [x_1, x_2, \dots, x_N]$ and $\Pi = [\Pi^1, \Pi^2, \dots, \Pi^M]$. Similar to t-SNE, we accomplish this using a gradient descent type algorithm. The ENS-T-SNE cost function (6) is defined as the sum of the t-SNE cost function evaluated at each of the 2D projections $\Pi^1 X, \Pi^2 X, \dots, \Pi^M X$.

$$\tilde{C}(X, \Pi) = \sum_{m=1}^M C(\Pi^m X) = \sum_{m=1}^M \sum_{i < j} p_{ij}^m \log \frac{p_{ij}^m}{q_{ij}^m}, \quad (11)$$

where C is the t-sne cost function. The gradients of \tilde{C} with respect to Y and $\Pi^1, \Pi^2, \dots, \Pi^M$ are then

$$\nabla_X \tilde{C}(X, \Pi^1, \Pi^2, \dots, \Pi^M) = \sum_{m=1}^M (\Pi^m)^T \nabla C(\Pi^m X) \quad (12)$$

and

$$\nabla_{\Pi^m} \tilde{C}(X, \Pi^1, \Pi^2, \dots, \Pi^M) = \nabla C(\Pi^m X) X^T. \quad (13)$$

As derived in [20], the gradient $\nabla C = \left[\frac{\partial C}{\partial y_1}, \frac{\partial C}{\partial y_2}, \dots, \frac{\partial C}{\partial y_N} \right]$ is given by

$$\frac{\partial C}{\partial y_i} = 4 \sum_j (p_{ij} - q_{ij})(y_i - y_j).$$

In its simplest form (full gradient and projected gradient descent), the update rules are

$$Y \mapsto Y + \mu \nabla_Y \tilde{C}(Y, \Pi^1, \Pi^2, \dots, \Pi^M)$$

and

$$\Pi^m \mapsto Q \left(\nu \nabla_{\Pi^m} \tilde{C}(Y, \Pi^1, \Pi^2, \dots, \Pi^M) \right),$$

where $\mu, \nu > 0$ are learning rates and Q maps a 2×3 matrix to its nearest orthogonal matrix.

In practice, we found that a combination of adaptive learning rate and stochastic gradient descent works the best in consistently avoiding local minima. To avoid flat solutions, we first optimize for the embedding Y while keeping the projections fixed (which are randomly chosen among the set of 2×3 orthogonal matrices). This algorithm is described in Algorithm 1.

3 Experiments on Synthetic Data

In this section we construct synthetic datasets which contain different types of clusters (captured in different subdimensions) by construction. Then we apply the ENS-t-SNE algorithm to test whether it can find an embedding in 3D Euclidean space that preserves the given multiple local structures.

Algorithm 1 Practical implementation of ENS-T-SNE

Input: $N \times N$ distances D^1, D^2, \dots, D^M , perplexity parameter Perp.
for perspectives $m = 1, 2, \dots, M$ **do**
 Compute $P^m = f(D^m, \text{Perp})$
end for
Assign initial values to $Y, \Pi = [\Pi^1, \Pi^2, \dots, \Pi^M], \mu, \nu$.
for batch size = $n/4, n/2$ **do**
 for $t = 1, 2, T$ **do**
 $Y = Y + \mu \nabla_Y^{ss} \tilde{C}(Y, \Pi)$
 $\mu = \mu + 1$
 end for
 for batch size = $n/4, n/2$ **do**
 for $t = 1, \dots, T$ **do**
 $Y = Y + \mu \nabla_Y^{ss} \tilde{C}(Y, \Pi)$
 $\Pi = \Pi + Q \left(\nu \nabla_{\Pi}^{ss} \tilde{C}(Y, \Pi) \right)$
 $\mu = \mu + 1$
 $\nu = \nu + 1$
 end for
 end for
Output: $Y, \Pi^1, \Pi^2, \dots, \Pi^M$.

3.1 Construction of Synthetic Data

In order to create a dataset with multiple perspectives, each containing multiple clusters, we propose the following procedure. Fix the number of points and the number of projections; for each projection fix the number of clusters, and the number of points corresponding to each cluster. For each perspective, randomly split the points between all the groups and define distances by assigning smaller within-cluster distances and larger between-cluster distances. The procedure is formally defined below.

Let the number of points be N and the number of perspectives be M . For each perspective set the number of clusters to NC_m , for $1 \leq m \leq M$, and the number of points corresponding to each cluster to $N_{c,m}$, where $1 \leq m \leq M$ and $1 \leq c \leq NC_m$. Note, that the total number N of points per perspective is a fixed constant and these points are in correspondence with each other. That is, $N = \sum_{c=1}^{NC_m} N_{c,m}$ for all $1 \leq m \leq M$.

For each perspective $1 \leq m \leq M$, the sample points with labels $1, 2, \dots, N$ are randomly assigned to one of NC_m clusters. That is, the sample point $1 \leq i \leq N$ will have labels $l_i^1, l_i^2, \dots, l_i^M$. Hence, two samples l_1 and l_2 may share the same label in some of the M perspectives, but are unlikely to share the same labels in all of them. Next, we create the distance matrix between the N datapoints as follows: The observed distance between points i, j for $1 \leq i, j, \leq N$ in each perspective m , where $1 \leq m \leq M$ is given by

$$D_{ij}^m = \begin{cases} d_{in}^m + \epsilon & \text{if } l_i^m = l_j^m \\ d_{out}^m + \epsilon & \text{otherwise} \end{cases} \quad (14)$$

where $\epsilon \sim N(0, \sigma^2)$ is a normal random variable with mean 0 and standard deviation σ^2 , d_{in}^m corresponds to within cluster distance for the m -th perspective and d_{out}^m corresponds to the outside cluster distances.

Since, the goal of ENS-t-SNE is to preserve local structures, this dataset suits its purpose and serves as a good example to show experimentally how the proposed ENS-t-SNE algorithm works. The aim is to show that similar to t-SNE for all of the perspectives, ENS-t-SNE preserves the local structures of the dataset, that is, each of the perspectives recovers the corresponding original clusters.

In Section 3.2 we demonstrate the application of ENS-t-SNE on several synthetic datasets created as described above.

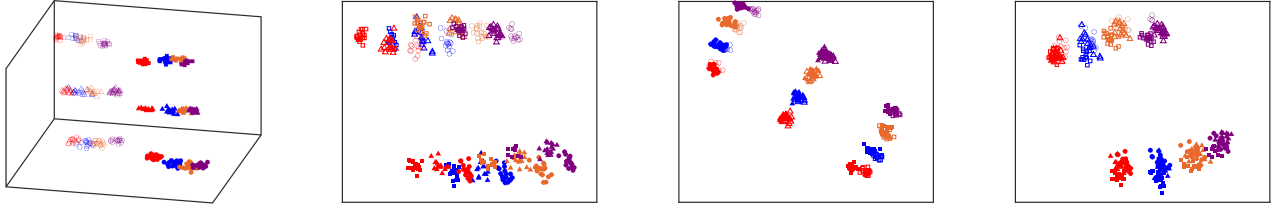


Fig. 2: ENS-t-SNE embedding of a clustered dataset, created according to Section 3.1 where the number of perspectives is $M = 3$, the number of datapoints is $N = 400$, and the number of clusters per perspective is $NC_1 = 2$, $NC_2 = 3$ and $NC_3 = 4$. The left figure shows a snapshot of the 3D ENS-t-SNE embedding and the next three figures show the 2D projections of the 3D ENS-t-SNE embedding. The original clusters are shown in color (red, blue, orange, and purple), shape (square, triangle and circle), and texture (filled or not). ENS-t-SNE algorithm is able to recover the clusters and create an embedding which respects all the different types of clusters.

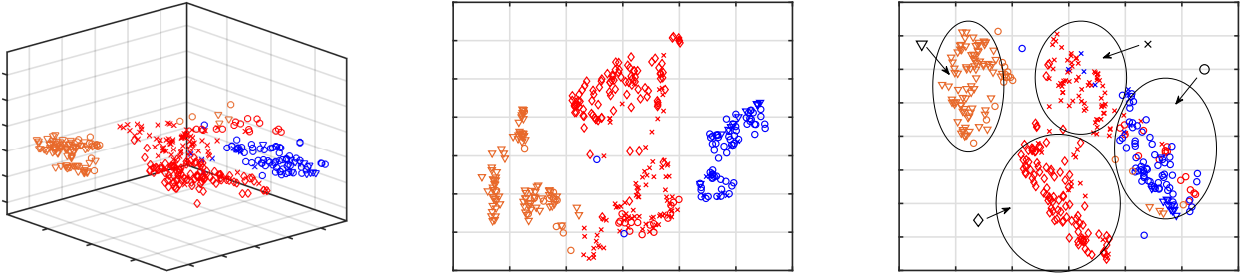


Fig. 3: Demonstration of the application of ENS-t-SNE algorithm on auto-mpg dataset. The left subfigure demonstrates a glimpse of the 3D ENS-t-SNE embedding of the dataset, the next two subfigures demonstrate the corresponding 2D projections of 3D ENS-t-SNE embedding. We use colors: red, blue, and orange to show the datapoints corresponding to cars with less or equal than four, more than four, and less or equal to 6 and more than 6 cylinders respectively. Furthermore, we use shapes: diamond, crosses, o, and triangles that represent cars whose weight is less than 25 percentile, between 25 and 50, between 50 and 75, and more than 75, respectively.

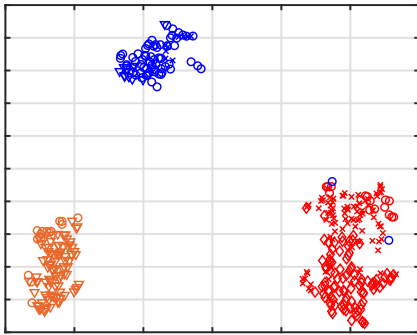


Fig. 4: 2D embedding of auto-mpg dataset by t-SNE. The colors and shapes are picked the same way as for Figure 3.

3.2 Application of ENS-t-SNE Algorithm on Clusters Dataset

We run the ENS-t-SNE, Algorithm 1, for datasets generated according to Section 3.1. For the first experiment, we fix the number of perspectives to be $M = 3$, the number of datapoints $N = 400$, the number of clusters per perspective $NC_m = 2$ for $1 \leq m \leq 3$. We create the distance matrices for each perspective by formula (14) described in Section 3.1 with $d_{in} = 1$ and $d_{out} = 2$ and $\sigma^2 = 0.1$. We run the ENS-t-SNE algorithm, summarized in Algorithm 1 and Section 2.1 for the distance

matrices and a fixed perplexity value of 100. The result are demonstrated in Figure 1.

To ease the visualization, we use colors, shape and texture. To show the original clusters for the first perspective, we use colors (blue and orange), for the second perspective, we use the shape (circles and squares), and for the third perspective, we use texture, filled and not filled; see Figure 1. We observe that ENS-t-SNE did a good job finding an embedding in 3D with 3 perspectives, such that for the first perspective the blue and orange datapoints are separated, for the second perspective, datapoints shown in circles and squares are separated, and for the third perspective, filled and not filled datapoints are separated. As expected, ENS-t-SNE split the data into multiple small clusters in 3D, but in such a way that for each 2D perspective, the ones with similar features in 3D overlap and create bigger clusters.

For the second experiment, we fix the number of perspectives to be $M = 3$, the number of datapoints $N = 400$, the number of clusters per perspective $NC_1 = 2$, $NC_2 = 3$, and $NC_3 = 4$. We create the distance matrices for each perspective by formula (14) described in Section 3.1 with $d_{in} = 1$ and $d_{out} = 2$ and $\sigma^2 = 0.1$. We run the ENS-t-SNE algorithm, Algorithm 1, for these distance matrices with perplexity value 100. The results are demonstrated in Figure 2.

To ease the visualization, we distinguish between the datapoints in the original clusters by color, shape, and texture. For the first perspective which has $NC_1 = 2$ clusters we use the texture (filled and not filled) to show the datapoints corresponding to original clusters. For the second perspective, which has $NC_2 = 3$ clusters we use 3 different shapes, squares,

circles and triangles to demonstrate the datapoints in original clusters. For the third perspective, where there are $NC_3 = 4$ original clusters, we use red, blue, orange and purple colors to distinguish between the original clusters. As we can see, ENS-t-SNE was able to find a 3D embedding which separates the data according to its clusters. Similar to the case where each perspective had only 2 clusters, for this case also ENS-t-SNE embedded the dataset in 3D with small clusters such that the projections on corresponding perspectives combined multiple small clusters and was able to preserve the desired local structure.

4 Experiments on Real-World Data

In this section we demonstrate the application of ENS-t-SNE algorithm on real-world datasets. We apply ENS-t-SNE algorithm to the auto-mpg dataset [9] to visualize different perspectives with different cluster information between the same set of cars; see Section 4.1. Then we apply the ENS-t-SNE algorithm to visualize the standard MNIST digits dataset, by considering the upper and lower parts of the digits; see Section 4.2.

4.1 Visualizing Different Perspectives of the Auto-mpg Dataset by ENS-t-SNE

The auto-mpg dataset from the UCI machine learning repository [9], provides data for 398 cars, each with the following 8 attributes: mpg, cylinders, displacement, horsepower, weight, acceleration, model year, origin. We split the characteristics of cars into two groups of three, such that the characteristics of each group are similar. We put (mpg, cylinders, displacement) in the first group and (horsepower, weight, acceleration) in the second group. The goal is to find an embedding of auto-mpg dataset into 3D such that one perspective shows the clusters of the dataset based on the first group and the second perspective shows the clusters of the dataset based on the second group.

In order to apply the ENS-t-SNE to auto-mpg dataset, for each of the groups mentioned above we compute the corresponding dissimilarity matrices by initially normalizing the dataset and computing the L_2 distances. We apply ENS-t-SNE algorithm for the above mentioned two distance matrices with perplexity value 30. The corresponding 3D embedding by ENS-t-SNE is demonstrated in Figure 3. In order to show the clusters in the obtained embedding, we use colors (red, blue, and orange) and shapes (diamond, triangle, square, and crosses).

To show the clusters in embedded dataset, we use the cylinders and the weights. We partition the total data into three groups based on the number of cylinders as follows: In the first group we place all the cars whose number of cylinders is not more than four, in the second group we put the cars whose number of cylinders are more than 4 and not more than 6 and in the third group we put the cars that have more than 6 cylinders. In Figure 3 the first group is colored in red, the second group is colored in blue and the third group is colored in orange. We further partition the dataset into four groups based on the weights according to 25, 50 and 75 quantiles. In Figure 3 the datapoints corresponding to the first group are shown in diamond shapes, the second group in crosses, the third group in circles and the fourth group in triangles.

Figure 3 demonstrates that the ENS-t-SNE was able to find an embedding of the dataset in 3D separating the data into several clusters. The first perspective groups together datapoints with the same colors, i.e., cars with similar numbers of cylinders are grouped together; see the second subfigure of Figure 3. The second perspective groups together datapoints with the same shapes, i.e., cars with similar weights are grouped together; see the third subfigure of Figure 3.

In Figure 3 we observe that although in the two perspectives cars are clustered according to corresponding dimensions (number of cylinders and weight), there are some exceptions.

For example, the blue outliers in the second (and also third) subfigure correspond to two exceptional cars which have low weights but higher number of cylinders (5 or 6).

Consider, for comparison, the standard t-SNE visualization of the same dataset in 2D; see Figure 4. The dominant factor for the embedding is the number of cylinders, resulting in three well-separated clusters in the embedding. Note, however, that the t-SNE embedding completely missed the weight information, as there is no pattern between the shapes. Contrast this with the ENS-t-SNE embedding, where both relationships (number of cylinders and weight) can be seen from the corresponding directions; see Fig. 3.

Applying ENS-t-SNE to similar datasets (with multiple interpretations) makes it possible to find a visualization that respects all interpretations. Furthermore, datapoints on the periphery of the clusters and outliers can be interpreted as datapoints that are very similar in one interpretation but completely different in others.

4.2 Visualizing MNIST Dataset by ENS-t-SNE

In this section we apply ENS-t-SNE to visualize the MNIST handwritten digit database [19]. The dataset contains 70,000 handwritten digits in greyscale, each of sizes 28×28 ; see examples from the dataset in Figure 5. The standard way of applying machine learning algorithms to the MNIST dataset is to vectorize the matrices corresponding to the greyscale pixel values of each digit and obtain a vector of size $28 \times 28 = 784$. Thus, each instance of the dataset can be viewed as a single datapoint in \mathbb{R}^{784} , with the idea being that points corresponding to the same digit should be close to each other. Dimensionality reduction techniques that aim to capture global distances (e.g., Principal Component Analysis and Multi-Dimensional Scaling) are known to perform poorly when embedding such data into 2D or 3D. Non-linear dimensionality reduction techniques that focus on local neighborhoods, such as t-SNE and UMAP, perform much better.



Fig. 5: Sample images from the MNIST dataset.

We apply ENS-t-SNE to embed the MNIST dataset (and similar datasets which require local neighborhood preservation) in 3D to capture the clusters corresponding to each digit. The idea is to define multiple distance/similarity measures between pairs of datapoints that would capture different properties/characteristics. As a simple initial example, each image can be divided into two parts: top and bottom; see Figure 6. We then compute the Frobenius norm, $\|A\|_F$ between the ma-

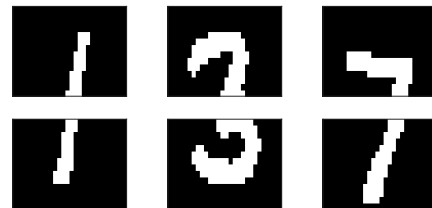


Fig. 6: MNIST dataset digits split into top and bottom parts.

trices corresponding to the greyscale pixel values of each image.

For a given matrix A , $\|A\|_F$ is defined as the square root of the sum of the squares of its elements and can be viewed as the vector L_2 norm of the vector of all elements of the matrix. Formally, for a matrix $A = (a_{i,j})_{i=1,j=1}^{m,n}$, its Frobenius norm is defined as:

$$\|A\|_F = \sqrt{\sum_{i=1}^m \sum_{j=1}^n a_{ij}^2}.$$

We now have two different sets of distance matrices: one corresponds to the top part of each image and the other corresponds to the bottom part of each image.

The idea behind this experiment is to apply ENS-t-SNE to a dataset with different perspectives, where some points are close to each other (in the same cluster) in one perspective, but are far from each other (in different clusters) in the other perspective. The ENS-t-SNE algorithm should place the points in 3D so that the desired properties are satisfied in the corresponding perspectives.

The distance matrices for the top and bottom parts of all datapoints are the inputs to the ENS-t-SNE algorithm. The results are different than those from the standard t-SNE applied on the original datapoints, as illustrated in Figures 8 and 7. The bottom view (the third subfigure of Fig. 7) shows that digits 1, 7 and 4 (sometimes 9, depending on the handwriting) are close to each other. This is expected since for most of these digits the bottom parts are nearly straight line segments oriented roughly the same way. However, since there is a significant difference in the top parts, the clusters are separated in 3D. Similarly, the pair of digits 3 and 5 are close in the bottom view and the digits 8 and 9 are close in the top view.

Comparing the standard t-SNE embedding in Figure 8, we can see that the ENS-t-SNE embedding managed to avoid some “errors”. For example in Figure 8, there are some 0s that appear within the cluster of 6s while that is not the case for ENS-t-SNE; see the left subfigure of Fig. 7.

In addition to the visual comparison between the MNIST dataset embedding obtained from ENS-t-SNE and the standard t-SNE, we also evaluate them using cluster accuracy [14, Section 10.6.3]. Specifically, given an embedding (from ENS-t-SNE or t-SNE) we apply K-MEANS clustering with 10 clusters and compare to the ground truth 10 clusters. For each embedding, finding the correct cluster labels is based on considering all re-orderings of the K-MEANS cluster labels and selecting the one that best matches the ground truth. After that, count the number of points that are correctly clustered and normalize it by the total number of points. The results suggest that ENS-t-SNE does as well or better than standard t-SNE: 0.539 for ENS-t-SNE in Fig. 7 vs. 0.478 for standard t-SNE in Fig. 8 (with higher scores corresponding to higher accuracy). The experiments were run for randomly chosen 1000 instances of MNIST dataset and averaged over 5 runs. In general, the accuracy is comparable, with a slight advantage to ENS-t-SNE.

5 Visualizing the Effect of Perplexity

The choice of perplexity parameter in t-SNE greatly affects the quality of achieved embedding; see [27]. Usually, smaller perplexity parameters produce visualizations that better reflect local distances between samples, however, when the perplexity is very small the algorithm fails to find a sufficiently good solution. Thus, finding an appropriate value of perplexity for which t-SNE would find the best possible embedding has been of research interest [8].

ENS-t-SNE can be used to visualize the differences between various perplexity parameters on the same given distance matrix. In practice, ENS-t-SNE seems to overcome the issue of not producing good results for smaller/larger-than-ideal perplexity value, as long as one of the perplexity values passed into ENS-t-SNE is sufficiently good. Specifically, we apply ENS-t-SNE

to the same set of distance matrices but with different perplexity values. The goal is to find an embedding of the dataset in 3D so that on the different projections it solves the t-SNE optimization with different perplexity values (but with the same distance matrix).

The problem formulation is as follows. Let D be an $N \times N$ distance matrix and $\text{perp}_1, \text{perp}_2, \dots, \text{perp}_M > 0$ be a list of perplexity parameters of interest. We wish to minimize the following cost function

$$\tilde{C}(X, \Pi; \text{perp}_1, \text{perp}_2, \dots, \text{perp}_M) = \sum_{m=1}^M C(\Pi^m X; \text{perp}_m) \quad (15)$$

where $Y \mapsto C(Y; \text{perp}_m)$ is the t-SNE cost function with perplexity parameter perp_m . Minimizing (15) is achieved using Algorithm (1) (varying the perplexity parameters while using the same distance matrix D).

In Figure 9, we show an application of ENS-t-SNE for a dataset that contains 2 clusters, constructed according to the model described in Section 3.1, with $M = 1$ and with $N = 400$ datapoints, using perplexity parameters equal to 3 and 100. The 3D embedding for the corresponding computed distance matrix, shown in the first row of Figure 9, and for the given two values of the perplexity parameter is the solution to problem (15). The two figures in the second row of Figure 9 show the projections of the 3D embedding that best represent the perspectives of this data set with perplexities 3 and 100.

As a way of comparison, we also compute the corresponding standard t-SNE 2D embeddings for the same distance matrix D with perplexities 3 and 100 (the last row of Figure 9). It is easy to see that standard t-SNE found the clusters when the perplexity was high and failed to find them when the perplexity was low, while ENS-t-SNE captured the clusters for both perplexity values. We note that whereas the images produced by ENS-t-SNE are projections of the same 3D embedding, the images produced by t-SNE are obtained independently.

6 Scalability of the Algorithm

In this section we consider the scalability of ENS-t-SNE with respect to the number of perspectives, the number of clusters per perspective, and the number of datapoints. In particular, the goal is to evaluate how the accuracy or the speed of ENS-t-SNE is affected as these parameters increase in value. The results indicate that the runtime of ENS-t-SNE scales reasonably well as these parameters increase. The accuracy decreases when the number of perspectives and clusters grows. However, if the number of perspectives is two the accuracy does not decrease as the number of clusters increase.

In order to measure the accuracy of the embedding for a dataset containing several clusters, we define the separation error as follows: For a 2D image containing two labels, the best linear classifier is found and the proportion of errors in this classification is returned. For a 2D image containing more than two labels, a linear classifier for every possible combination of two labels is computed, and the average proportion of errors between all combinations is returned. For a 3D embedding with multiple perspectives, with each image having two or more labels, the separation error in each image is computed and the average is returned.

To check the scalability of the proposed ENS-t-SNE algorithm we create datasets as described in Section 3.1. We consider $N = 400$ datapoints and vary the number of perspectives $M = 2, 3, \dots, 10$, making sure that each perspective has $NC_m = 2$ identifiable clusters in it. We then apply ENS-t-SNE for each of these datasets using perplexity values 40, 80, 160, 240 and report the results in the top left subfigure of Figure 10. The x-axis of the top left subfigure of Figure 10 shows the number of perspectives and the y-axis shows the separation error. The results indicate that for a small number of perspectives (2,3)

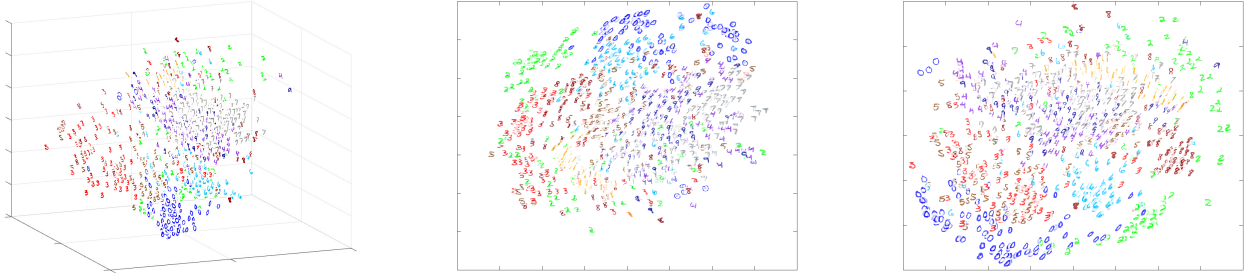


Fig. 7: Application of ENS-t-SNE to the 1000 instances from the MNIST dataset with perplexity value 500. The left subfigure demonstrates the 3D embedding computed by ENS-t-SNE. The middle subfigure demonstrates the projection of the 3D embedding onto the view that corresponds to the distance matrix constructed from the upper parts of the digits. The right subfigure demonstrates the projection of the 3D embedding onto the view that corresponds to the distance matrix constructed from the lower parts of the digits.

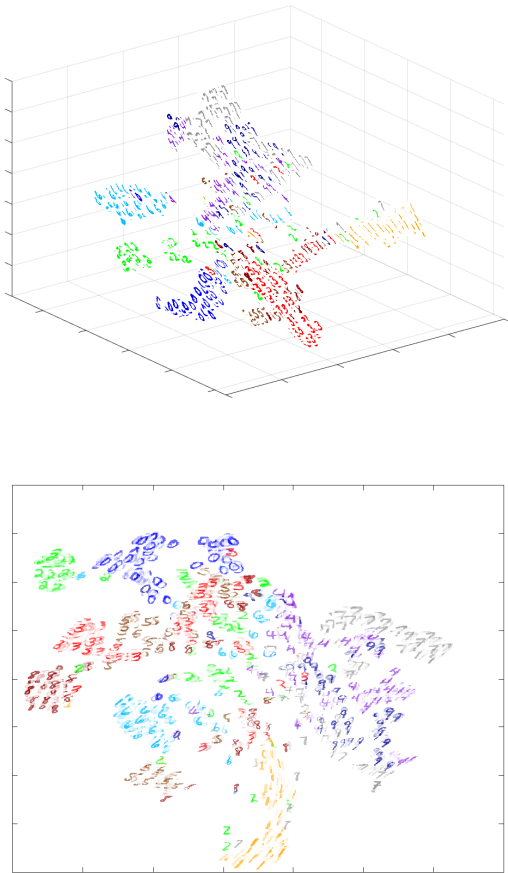


Fig. 8: 3D (top) and 2D (bottom) embedding obtained by t-SNE of a subset with 1000 datapoints from the MNIST dataset.

the separation error is small and as the number of perspective increases the error grows.

Next, we test the scalability of the algorithm as the number of clusters per perspectives increases. We create the datasets in a similar fashion setting $N = 400$, $M = 2, 3$, and varying the number of clusters per perspective $NC_m = 2, 3, \dots, 10$. We run ENS-t-SNE with perplexity values 40, 80, 160, 240 and report the separation error in the top right subfigure of Fig-

ure 10. The results indicate that as the number of clusters increase for 3 perspectives, the separation error grows, while for 2 perspectives the separation error is stable.

We continue by analyzing the influence of the number of datapoints on the running time of the algorithm. For this purpose, we create datasets containing clusters according to Section 3.1. We set the number of perspectives $M = 2, 3$ and the number of clusters per perspective $NC_m = 2$, while varying the total number of datapoints N from 200 to 1800 in increments of 200. We run ENS-t-SNE for these datasets with perplexity value $0.2 * N$ and report the running time as a function of N in the bottom left subfigure of Figure 10. The results indicate a steady increase in running time as the number of datapoints and the number of perspectives grow.

The final experiment tests the effect of the number of perspectives on the accuracy of the algorithm. We generate the dataset as follows: We uniformly distribute 1000 points in a solid 3D ball, and randomly select several perspectives. We label each point in each perspective according to on which side of the perspective the points fall into. The perplexity is fixed to 600 and the number of perspectives vary from 2 to 10. We report the separation error vs the number of perspectives in the bottom right subfigure of Figure 10. The results indicate that when there are no forced clusters, the algorithm has more freedom to separate the data into parts that respect the original label assignment. Thus, the separation error is more stable.

7 Conclusions

We described ENS-t-SNE, a generalization of t-SNE, where instead of one distance matrix we consider multiple distances simultaneously. The algorithm computes an embedding of the dataset in 3D and a set of perspectives/projections, so that the local distances of each distance matrix is preserved in the corresponding projection.

As the main part of the paper describes the proposed ENS-t-SNE algorithm (from the idea to the implementation), the quantitative and qualitative evaluation is just sketched out here. Nevertheless, several different types of experiments, on synthetic and real-world datasets, indicate that ENS-t-SNE can indeed simultaneously capture multiple different types of relationships defined on the same set of high-dimensional objects.

Interesting future work includes combining the ENS-t-SNE algorithm with the MPSE algorithm of Hossain et al. [15] to simultaneously embed a dataset using local measure from one perspective (e.g., t-SNE) and a global measure for the other perspective (e.g., MDS). Similarly, other dimensionality reduction methods such as UMAP [22] can be generalized to simultaneously capture multiple aspects, or combined with ENS-t-SNE and MPSE to balance local and global distance preservation.

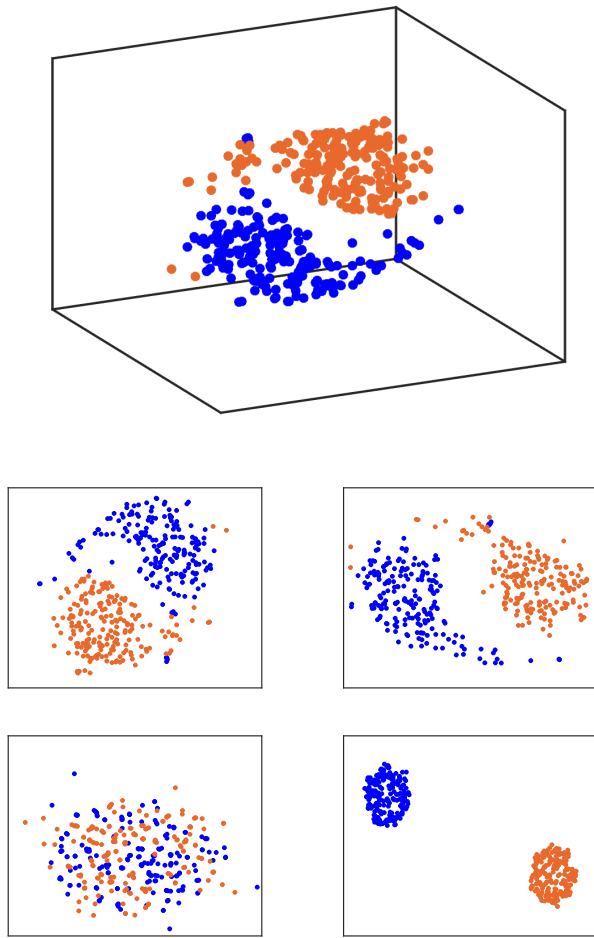


Fig. 9: Comparison of the ENS-t-SNE visualization of a dataset with perplexities 3 and 100 and the corresponding t-SNE visualizations. The dataset contains 400 samples that form two clusters, as colored. The top image shows a glimpse of the 3D ENS-t-SNE embedding. The middle two images show the two projections of the 3D ENS-t-SNE embedding, the left corresponding to perplexity 3 and the right corresponding to perplexity 100. The bottom two images are t-SNE visualizations of the same distances using perplexity 3 (left) and perplexity 100 (right).

References

- [1] S. Bai, X. Bai, L. J. Latecki, and Q. Tian. Multidimensional scaling on multiple input distance matrices. In *Thirty-First AAAI Conference on Artificial Intelligence*, 2017.
- [2] M. Belkin and P. Niyogi. Laplacian eigenmaps and spectral techniques for embedding and clustering. In *Advances in Neural Information Processing Systems 14*, pp. 585–591. MIT Press, 2001.
- [3] A. C. Belkina, C. O. Ciccolella, R. Anno, R. Halpert, J. Spidlen, and J. E. Snyder-Cappione. Automated optimized parameters for t-distributed stochastic neighbor embedding improve visualization and analysis of large datasets. *Nature communications*, 10(1):1–12, 2019.
- [4] N. v. Beusekom, W. Meulemans, and B. Speckmann. Simultaneous matrix orderings for graph collections. *IEEE Transactions on Visualization and Computer Graphics*, pp. 1–1, 2021. doi: 10.1109/TVCG.2021.3114773
- [5] T. Bläsius, S. G. Kobourov, and I. Rutter. Simultaneous embedding of planar graphs. In R. Tamassia, ed., *Handbook of Graph*

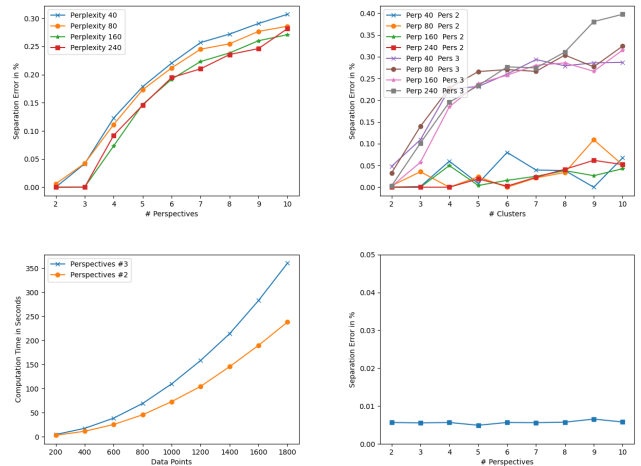


Fig. 10: Demonstration of the scalability of the ENS-t-SNE algorithm. The top left subfigure shows the separation error for 400 samples with two clusters in each perspective (independent from each other), varying the number of perspectives and the perplexity values. The top-right subfigure shows the separation error for 400 samples with multiple clusters in each perspective (independent from each other), varying the number of perspectives and the perplexity values. The bottom left subfigure shows the running time for 2 and 3 perspectives, for 2 and 3 clusters, while varying the sample sizes. The bottom right subfigure shows the separation error for 1000 samples uniformly distributed in a solid 3D ball, with perspectives chosen at random, and labels chosen depending on which side of each 2D image each point falls into. The perplexity is fixed to 600 and the number of perspectives vary.

Drawing and Visualization, pp. 349–381. CRC Press, 2013.

- [6] L. Bottou. Large-scale machine learning with stochastic gradient descent. In *Proceedings of COMPSTAT'2010*, pp. 177–186. Springer, 2010.
- [7] P. Brass, E. Cenek, C. A. Duncan, A. Efrat, C. Erten, D. P. Ismailescu, S. G. Kobourov, A. Lubiw, and J. S. Mitchell. On simultaneous planar graph embeddings. *Computational Geometry*, 36(2):117–130, 2007.
- [8] Y. Cao and L. Wang. Automatic selection of t-sne perplexity. *CoRR*, abs/1708.03229, 2017.
- [9] D. Dua and C. Graff. UCI machine learning repository, 2017.
- [10] E. R. Gansner, Y. Koren, and S. North. Graph drawing by stress majorization. In *International Symposium on Graph Drawing*, pp. 239–250. Springer, 2004.
- [11] B. Ghojogh, A. Ghodsi, F. Karray, and M. Crowley. Stochastic neighbor embedding with gaussian and student-t distributions: Tutorial and survey. *CoRR*, abs/2009.10301, 2020.
- [12] B. Ghojogh, A. Ghodsi, F. Karray, and M. Crowley. Uniform manifold approximation and projection (UMAP) and its variants: Tutorial and survey. *CoRR*, abs/2109.02508, 2021.
- [13] L. Grilli, S.-H. Hong, G. Liotta, H. Meijer, and S. K. Wismath. Matched drawability of graph pairs and of graph triples. *Computational Geometry*, 43(6-7):611–634, 2010.
- [14] J. Han, J. Pei, and M. Kamber. *Data mining: concepts and techniques*. Elsevier, 2011.
- [15] M. I. Hossain, V. Huroyan, S. G. Kobourov, and R. Navarrete. Multi-perspective, simultaneous embedding. *IEEE Trans. Vis. Comput. Graph.*, 27(2):1569–1579, 2021. doi: 10.1109/TVCG.2020.3030373
- [16] I. T. Jolliffe. *Principal Component Analysis*. Springer Series in Statistics. Springer, 1986. doi: 10.1007/978-1-4757-1904-8
- [17] S. Kanaan Izquierdo, A. Ziyatdinov, M. A. Burgueño, and A. Perera Lluna. Multiview: a software package for multiview pattern recognition methods. *Bioinformatics*, (bty1039):1–3,

- 2018.
- [18] J. B. Kruskal. Multidimensional scaling by optimizing goodness of fit to a nonmetric hypothesis. *Psychometrika*, 29(1):1–27, 1964.
 - [19] Y. LeCun and C. Cortes. MNIST handwritten digit database. 2010.
 - [20] L. v. d. Maaten and G. Hinton. Visualizing data using t-sne. *Journal of machine learning research*, 9(11):2579–2605, 2008.
 - [21] L. McInnes and J. Healy. UMAP: uniform manifold approximation and projection for dimension reduction. *CoRR*, abs/1802.03426, 2018.
 - [22] L. McInnes, J. Healy, N. Saul, and L. Großberger. UMAP: uniform manifold approximation and projection. *J. Open Source Softw.*, 3(29):861, 2018. doi: 10.21105/joss.00861
 - [23] S. Mitra, S. Saha, and M. Hasanuzzaman. Multi-view clustering for multi-omics data using unified embedding. *Scientific reports*, 10(1):1–16, 2020.
 - [24] T. Rodosthenous, V. Shahrezaei, and M. Evangelou. Multi-view data visualisation via manifold learning. *arXiv preprint arXiv:2101.06763*, 2021.
 - [25] R. N. Shepard. The analysis of proximities: multidimensional scaling with an unknown distance function. *Psychometrika*, 27(2):125–140, 1962.
 - [26] L. van der Maaten. Accelerating t-sne using tree-based algorithms. *Journal of Machine Learning Research*, 15(93):3221–3245, 2014.
 - [27] M. Wattenberg, F. Viégas, and I. Johnson. How to use t-sne effectively. *Distill*, 1(10):e2, 2016.
 - [28] T. Xia, D. Tao, T. Mei, and Y. Zhang. Multiview spectral embedding. *IEEE Trans. Syst. Man Cybern. Part B*, 40(6):1438–1446, 2010. doi: 10.1109/TSMCB.2009.2039566
 - [29] B. Xie, Y. Mu, and D. Tao. m-SNE: Multiview stochastic neighbor embedding. In K. W. Wong, B. S. U. Mendis, and A. Bouzerdoum, eds., *Neural Information Processing. Theory and Algorithms*, pp. 338–346. Springer Berlin Heidelberg, Berlin, Heidelberg, 2010.
 - [30] B. Xie, Y. Mu, D. Tao, and K. Huang. m-SNE: Multiview stochastic neighbor embedding. *IEEE Transactions on Systems, Man, and Cybernetics, Part B (Cybernetics)*, 41(4):1088–1096, 2011. doi: 10.1109/TSMCB.2011.2106208